AGU ADVANCING EARTH AND SPACE SCIENCE

Geophysical Research Letters

RESEARCH LETTER
10.1029/2021GL094252

Estimating Ice Discharge at Greenland's Three Largest Outlet Glaciers Using Local Bedrock Uplift

Karina Hansen[1], Martin Truffer[2], Andy Aschwanden[2,3], Kenneth Mankoff[3], Michael Bevis[4], Angelika Humbert[5], Michiel R. van den Broeke[6], Brice Noël[6], Anders Bjørk[7], William Colgan[3], Kurt H. Kjær[8], Surendra Adhikari[9], Valentina Barletta[1], and Shfaqat A. Khan[1]

[1]DTU Space, Technical University of Denmark, Kongens Lyngby, Denmark, [2]Geophysical Institute, University of Alaska Fairbanks, Fairbanks, AK, USA, [3]Department of Glaciology and Climate, Geological Survey of Denmark and Greenland, Copenhagen, Denmark, [4]School of Earth Sciences, Ohio State University, Colombus, OH, USA, [5]Alfred-Wegener-Institut Helmholtz Zentrum für Polar- und Meeresforschung, Germany and University of Bremen, Bremerhaven, Germany, [6]Institute for Marine and Atmospheric Research Utrecht, Utrecht University, Utrecht, The Netherlands, [7]Department of Geosciences and Natural Resources, University of Copenhagen, Copenhagen, Denmark, [8]Centre for GeoGenetics, Globe Institute, University of Copenhagen, Copenhagen, Denmark, [9]Jet Propulsion Laboratory, California Institute of Technology, Pasadena, CA, USA

Key Points:

- A novel method to estimate dynamic ice loss of Greenland's three largest outlet glaciers, Jakobshavn, Kangerlussuaq, and Helheim glacier
- Dynamic thinning/thickening occurs 0.87 ± 0.07 years before speedup/slowdown at Jakobshavn Isbræ
- A similar time lag between change in uplift rate and flow speed change allows us to predict future ice discharge from past uplift

Supporting Information:

Supporting Information may be found in the online version of this article.

Correspondence to:

S. A. Khan,
abbas@space.dtu.dk

Citation:

Hansen, K., Truffer, M., Aschwanden, A., Mankoff, K., Bevis, M., Humbert, A., et al. (2021). Estimating ice discharge at Greenland's three largest outlet glaciers using local bedrock uplift. *Geophysical Research Letters*, *48*, e2021GL094252. https://doi.org/10.1029/2021GL094252

Received 11 MAY 2021
Accepted 29 JUN 2021

Abstract We present a novel method to estimate dynamic ice loss of Greenland's three largest outlet glaciers: Jakobshavn Isbræ, Kangerlussuaq Glacier, and Helheim Glacier. We use Global Navigation Satellite System (GNSS) stations attached to bedrock to measure elastic displacements of the solid Earth caused by dynamic thinning near the glacier terminus. When we compare our results with discharge, we find a time lag between glacier speedup/slowdown and onset of dynamic thinning/thickening. Our results show that dynamic thinning/thickening on Jakobshavn Isbræ occurs 0.87 ± 0.07 years before speedup/slowdown. This implies that using GNSS time series we are able to predict speedup/slowdown of Jakobshavn Isbræ by up to 10.4 months. For Kangerlussuaq Glacier the lag between thinning/thickening and speedup/slowdown is 0.37 ± 0.17 years (4.4 months). Our methodology and results could be important for studies that attempt to model and understand mechanisms controlling short-term dynamic fluctuations of outlet glaciers in Greenland.

Plain Language Summary A wide range of sensors and methods have been used to study the changes of the Greenland Ice Sheet, including satellite gravimetry, altimetry, and the input-output method. Here, we present a novel fourth method to estimate dynamic ice loss of Greenland's three largest outlet glaciers: Jakobshavn Isbræ, Kangerlussuaq Glacier, and Helheim Glacier. We use Global Navigation Satellite System (GNSS) stations attached to bedrock to measure rise of land masses caused by ongoing ice mass loss near the glacier terminus. When we compare our results with ice discharge, we find a time lag between glacier speedup/slowdown and onset of dynamic induced thinning/thickening. Our results show that dynamic thinning/thickening on Jakobshavn Isbræ occurs 0.87 ± 0.07 years before speedup/slowdown. This implies that using GNSS uplift time series we are able to predict ice flow speedup/slowdown of Jakobshavn Isbræ by up to 10 months. For Kangerlussuaq Glacier and Helheim Glacier the lag between thinning/thickening and speedup/slowdown is 0.37 ± 0.17 years (4.4 months) and 0.03 ± 0.16 years, respectively. Our methodology and results could be important for studies that attempt to model and understand mechanisms controlling short-term dynamic fluctuations of outlet glaciers in Greenland.

1. Introduction

The mass loss of the Greenland Ice Sheet (GrIS) has been accelerating during the last quarter of a century (Bamber et al., 2018; Mouginot et al., 2019; Shepherd et al., 2020) with rapid and record-high ice-sheet-wide losses in 2012 and 2019 (Nghiem et al., 2012; Sasgen et al., 2020). A wide range of sensors and methods has been used to study the changes of the GrIS, including satellite gravimetry, altimetry, and the input-output method (IOM). Satellite gravity measurements from the Gravity Recovery and Climate Experiment (GRACE/-FO) can be converted into mass change (Chen et al., 2006; Sasgen et al., 2020; Velicogna &

Wahr, 2006). Airborne and satellite altimetry directly measure changes in ice surface heights and provide ice volume changes (Helm et al., 2014; Khan, Kjær et al., 2014; Pritchard et al., 2009). The IOM method depends on the discharge of ice through a flux gate (Rignot & Kanagaratnam, 2006) and surface mass balance (van den Broeke et al., 2016). Each of these methods has strengths and weaknesses. GRACE/-FO provides solutions at high temporal (monthly) but limited spatial resolution, and is thus not suitable to study individual glaciers (Barletta et al., 2013). Satellite and airborne altimetry provide high spatial resolution but limited temporal sampling (monthly to annual) (Khan, Kjeldsen et al., 2014; Schenk et al., 2014). IOM has the advantage that it identifies the physical processes responsible for the mass changes; it provides weekly solutions but is available only since 2016 (King et al., 2020; Mankoff et al., 2020) while yearly solutions are available since 1972 (Mouginot et al., 2019). However, while GRACE provides direct estimates of mass changes, both altimetry and IOM methods need several models and/or a priori knowledge to derive the ice mass changes, resulting in relatively high uncertainties in ice mass loss estimates.

Here, we present a novel method to estimate dynamic ice loss from direct observations of uplift of the elastic lithosphere using Global Navigation Satellite System (GNSS) stations attached to bedrock. GNSS stations are uplifting due to a combination of Glacial Isostatic Adjustment (GIA, caused by past ice-ocean mass exchange) and Earth's near instantaneous elastic response to present-day ice mass changes (Bevis et al., 2012). The Earth's elastic response can be isolated by applying a GIA correction. The magnitude of the elastic response to ice loss decreases with increasing distance from the ice loss center (Adhikari et al., 2017; Wahr et al., 2013), which means GNSS stations located near the center of ice loss will experience more uplift than GNSS stations further away. The Earth's elastic response is due to a combination of dynamic thinning of glaciers and surface mass balance (SMB) processes. However, these two contributors to surface elevation changes have different spatial patterns. Dynamic thinning is typically largest near the glacier terminus and along the main flowline and declines rapidly inland (Khan et al., 2020; Khazendar et al., 2019), while SMB-induced thinning has a much larger wavelength as SMB anomalies typically have a larger footprint. Earth's elastic response due to dynamic thinning can be isolated by applying a correction for SMB-induced elastic uplift. Therefore, a GNSS station located near a glacier front can sense and reveal the dynamic mass changes of that particular glacier. Here, we take advantage of GNSS stations located next to a major outlet glacier undergoing dynamic changes.

The major advantage of using GNSS data is the very high temporal resolution (daily) of elastic uplift estimates, caused by daily mass loss variability of the nearby glacier. In general, GNSS data may reveal short-term fluctuation of mass and significantly improve our understanding of glacier dynamics at daily timescales (Adhikari et al., 2017; Khan et al., 2010). Here, we focus on GNSS data from stations near Greenland's three largest outlet glaciers, Jakobshavn Isbræ (Sermeq Kujalleq, JI), Kangerlussuaq Glacier (KG), and Helheim Glacier (HG). We develop a relation between GNSS uplift and accumulated ice discharge for each glacier to examine recent ice variability.

2. Data and Methods

2.1. GNSS Data

To estimate GNSS site coordinates, we use the Gipsy X software package version GipsyX-1.3 developed at the Jet Propulsion Laboratory (JPL) and released in December 2019 (Bertiger et al., 2020). We use JPL final orbit products which include satellite orbits, satellite clock parameters, and Earth orientation parameters. The orbit products take the satellite antenna phase center offsets into account. The atmospheric delay parameters are modeled using the Vienna Mapping Function 1 (VMF1) with VMF1grid nominals (Boehm et al., 2006). Corrections are applied to remove the solid Earth tide and ocean tidal loading. The amplitudes and phases of the main ocean tidal loading terms are calculated using the Automatic Loading Provider (http://holt.oso.chalmers.se/loading/) applied to the FES2014b (Carrère et al., 2016) ocean tide model, including correction for center of mass motion of the Earth due to the ocean tides. The site coordinates are computed in the IGS14 frame (Altamimi et al., 2016).

Here, we use GNSS data from three sites located on bedrock near the margin of JI, KG, and HG. Figures 1a–1c shows the locations of the GNSS sites (red dots). KAGA is located near JI, KUAQ near KG, and HEL2 near HG. The blue curves in Figure 2 (left panels) show weekly solutions of bedrock uplift at KAGA,

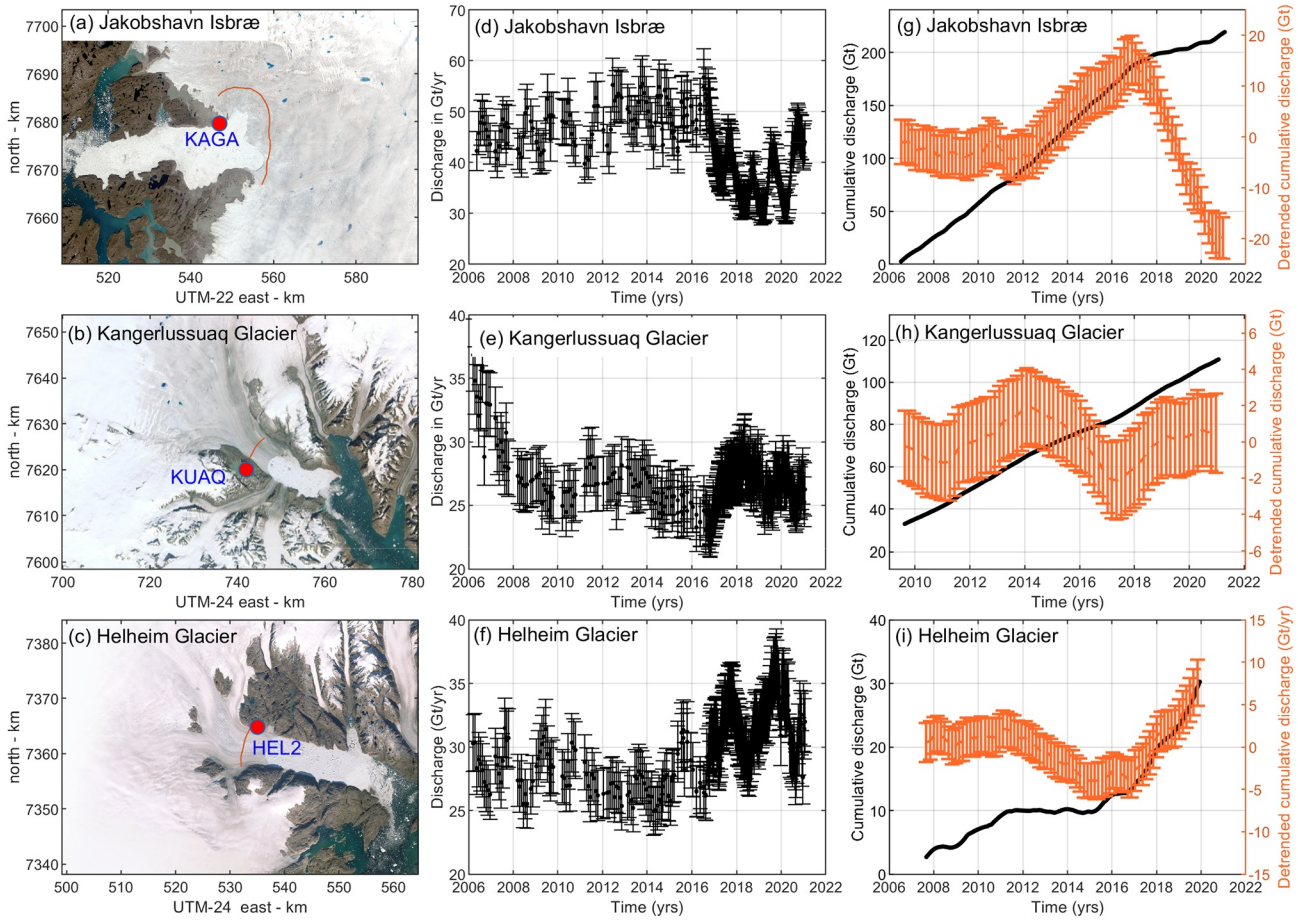

Figure 1. (a) Jakobshavn Isbræ and the location of flux gate (red curve) and GNSS station KAGA (red dot). (b) Kangerlussuaq Glacier and location of flux gate (red curve) and GNSS station KUAQ (red dot). (c) Helheim Glacier and location of flux gate (red curve) and GNSS station HEL2 (red dot). Time series of ice discharge from (d) JI, (e) KG, and (f) HG. Black curve denotes time series of cumulative ice discharge (left axis) from (g) JI, (h) KG, and (j) HG. Orange curve denotes time series of detrended cumulative ice discharge (right axis) from (g) JI, (h) KG, and (i) HG.

KUAQ, and HEL2, respectively. To isolate the uplift associated with ice dynamic processes, we must account for the uplift associated with SMB processes. The red curves in Figure 2 (left panels) denote estimated elastic uplift caused by SMB anomalies. This SMB correction is described in the following section.

2.1.1. Surface Mass Balance Correction

We use surface mass balance output products from the Regional Atmospheric Climate Model (RACMO2.3p2) at 5.5 km horizontal resolution statistically downscaled to 1 km resolution (Noël et al., 2018, 2019). SMB uncertainty has been previously estimated using the bias between modeled and observed SMB. We use an accumulation zone uncertainty of 17 mm w.e./yr and an ablation zone uncertainty of 70 mm w.e./yr (Noël et al., 2019).

To estimate "elastic uplift due to SMB," we integrate this SMB product over the drainage catchment of each glacier, and then remove the mean 1961–1990 to obtain SMB mass anomalies. Next, we convolve SMB mass anomalies with the Green's functions derived by Wang et al. (2012) for elastic Earth model iasp91 with refined crustal structure from Crust 2.0. The blue curves in Figure 2 (left panels) denote GNSS observed uplift corrected for "elastic uplift due to SMB," which we for simplicity denote as "elastic uplift due to ice dynamics." In Figure 2 (right panel), we detrend the "elastic uplift due to ice dynamics" weekly solutions by fitting and removing a linear term and yearly term, allowing us to ignore, for example, glacial isostatic adjustment correction.

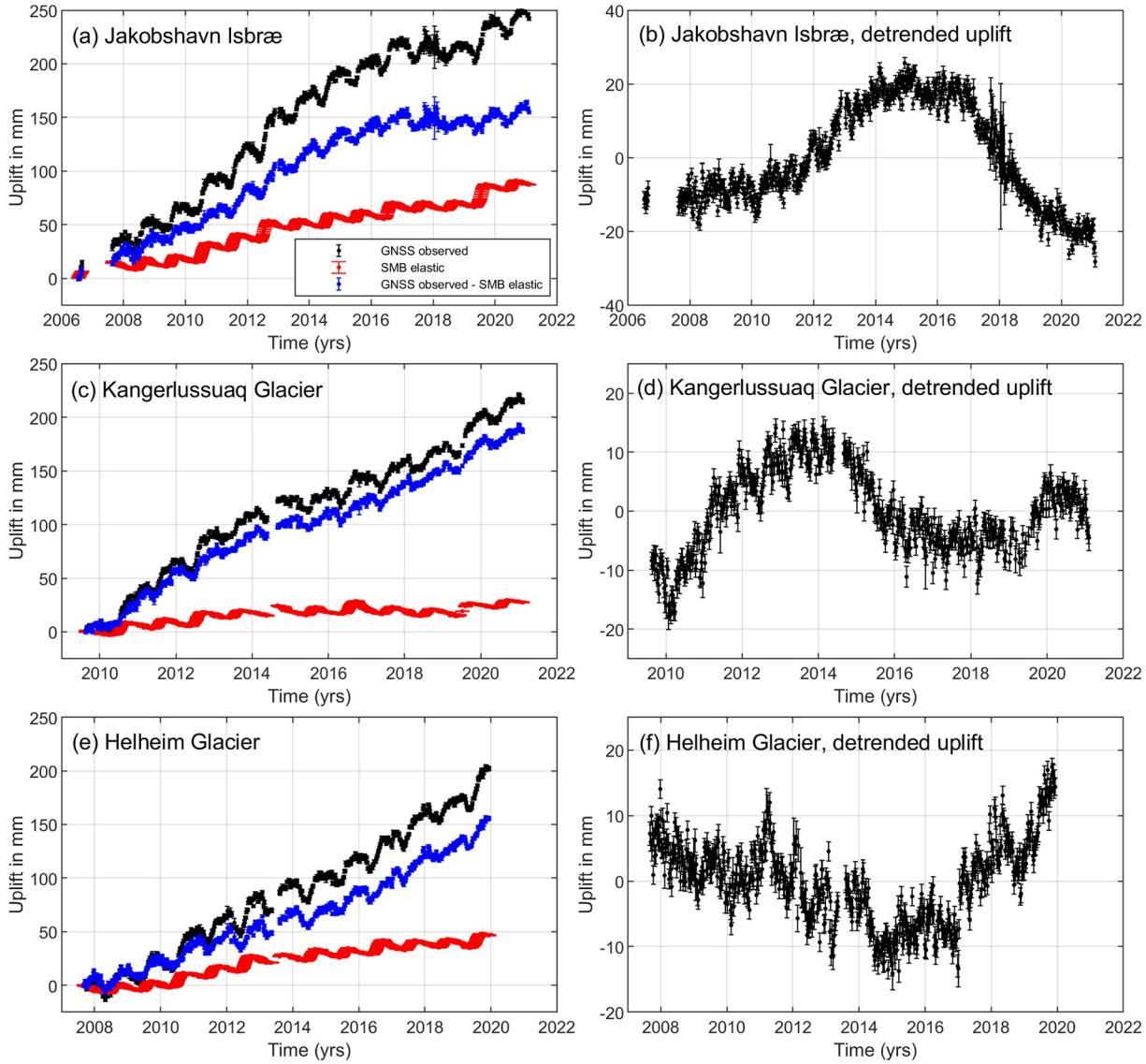

Figure 2. (a) Time series of weekly uplift solution at KAGA (black curve). Time series of elastic uplift due to SMB anomalies at KAGA (red curve). Observed uplift subtracted elastic uplift due to SMB (blue curve). (c) Same as (a) but for KUAQ. (f) Same as (a) but for HEL2. (b) Detrended observed uplift subtracted elastic uplift due to SMB at KAGA. (d) Detrended observed uplift subtracted elastic uplift due to SMB at KUAQ. (f) Detrended observed uplift subtracted elastic uplift due to SMB at HEL2.

2.1.2. Uncertainties of the Elastic Uplift Due to Ice Dynamics

We construct weekly averages of the daily vertical solutions shown to take the temporally correlated (non-Gaussian) noise into account. We use the root mean square (rms) of those averages to represent their uncertainties that we denote $\sigma_{\text{up\_GPS}}$. To estimate uncertainties of the elastic uplift due to SMB, we convolve SMB uncertainty with the Green's functions and denote these uncertainties as $\sigma_{\text{up\_SMB}}$. The total uncertainties of the "elastic uplift due to ice dynamics" (blue curves in Figures 2a, 2c and 2e) are $\sigma_{\text{elas}} = \sqrt{\sigma^2_{\text{up\_GPS}} + \sigma^2_{\text{up\_SMB}}}$.

The resulting uncertainty σ_{elas} is dominated by the GNSS data uncertainty which is typically1.5–2.0 mm, while the magnitude of $\sigma_{\text{up\_SMB}}$ is about 0.4 mm.

Table 1
Parameter k, t_0, and Trend for JI, KG, and HG

Glacier	k [Gt/mm]	t_0 [years]	Trend of dynamic ice loss [Gt/yr]
JI	0.67 ± 0.01	0.87 ± 0.07	16.2
KG	0.13 ± 0.01	0.37 ± 0.17	6.7
HG	0.46 ± 0.01	0.03 ± 0.16	1.6

2.2. Ice Discharge and Uncertainties

We use JI, KG, and HG solid ice discharge from December 2006 to 2020. Discharge is calculated across flux gates, from ice thickness (Morlighem et al., 2017) updated to account for surface elevation change (Khan et al., 2016), ice surface velocity (Solgaard et al., 2021), and an assumed ice density of 917 kg/m^3 (Mankoff et al., 2020). Gates are placed ∼5 km upstream from the terminus and limited to ice flowing >100 m/yr, based on the average 2015, 2016, and 2017 winter velocity as provided by MEaSUREs (Joughin et al., 2018). The largest uncertainties in estimated ice discharge are associated with ice thickness uncertainties (Morlighem et al., 2017), and ice density uncertainty due to crevasses.

Figures 1a–1c shows the location of flux gates for each glacier and Figures 1d–1f shows the ice discharge rate in Gt/yr. To estimate dynamic ice loss, we estimate cumulative discharge of each glacier and remove the associated basin-wide mean 1961–1990 SMB, which is typically assumed to characterize a near-equilibrium period (King et al., 2020). We estimate a 1961–1990 basin-wide mean SMB using RACMO2.3p2 of 29.9 Gt/yr for JI, 19.5 Gt/yr for KG, and 26.5 Gt/yr for HG. Figures 1g–1i shows the dynamic ice loss (black curve) and the detrended dynamic ice loss (orange curve). To detrend the dynamic ice loss, we fit and remove a linear term and yearly term.

2.3. Airborne and Satellite Laser Altimetry

To assess elevation changes of the ice surface over JI, we use repeat laser altimetry surveys from NASA's Airborne Topographic Mapper (ATM) flights during 2006–2019 (Studinger, 2014). The airborne altimetry measurements over the ice were conducted from March to May during annual campaigns as part of NASA's Operation IceBridge. NASA ended its Operation IceBridge measurement over Greenland in spring 2019. To assess ice surface elevation changes during 2019–2020, we use Land Ice Along-Track Height Product (ATL06) from ICESat-2 (Ice, Cloud, and land Elevation Satellite 2) launched on September 15, 2018, as part of NASA's Earth Observing System (Smith et al., 2020). To estimate elevation changes from 2019 to 2020, we use surface elevations from January to mid-May for 2019 and difference with surface elevations from January to mid-May for 2020.

3. Dynamic Ice Loss From GNSS Uplift

The time series of detrended dynamic ice loss from flow speed (Figure 1 right panels) represent dynamic changes of JI, KG, and HG, respectively. We denote the time series of detrended dynamic ice loss from flow speed as $D(t)$, where t is time. However, the time series of detrended elastic uplift (Figure 2 right panels) represent changes in uplift due to ice dynamics at JI, KG, and HG. We denote $U(t)$ as time series of detrended elastic uplift due to dynamic ice loss. For both detrended time series, positive anomalies reflect periods of higher than normal ice dynamic mass loss. We detrend the dynamic ice loss and uplift time series over a common time period at each glacier, so the anomalies in each record are equivalent. Estimated trends removed from dynamic ice loss time series are listed in Table 1.

$U(t)$ is the detrended elastic uplift due to dynamic ice loss and depends on the distance between the GNSS site and the center of the area undergoing dynamic thinning. Here, we assume that this distance is constant over the time period of comparison. $D(t)$ is the detrended discharge at the flux gate and depends on the flux gate location (see Text S1), ice flow speed and ice thickness at the flux gate. For a glacier that thins and speeds up simultaneously, we can assume a simple linear relation between $U(t)$ and $D(t)$. However, if the speed-up lags the thinning as a consequence of the thinning, we have to introduce a time lag between $U(t)$ and $D(t)$. Based on our timeseries we assume a simple linear relation between $U(t)$ and $D(t)$ with a time lag between the two time-series,

$$D\left(t\right) = k * U\left(t - t_0\right) \quad (1)$$

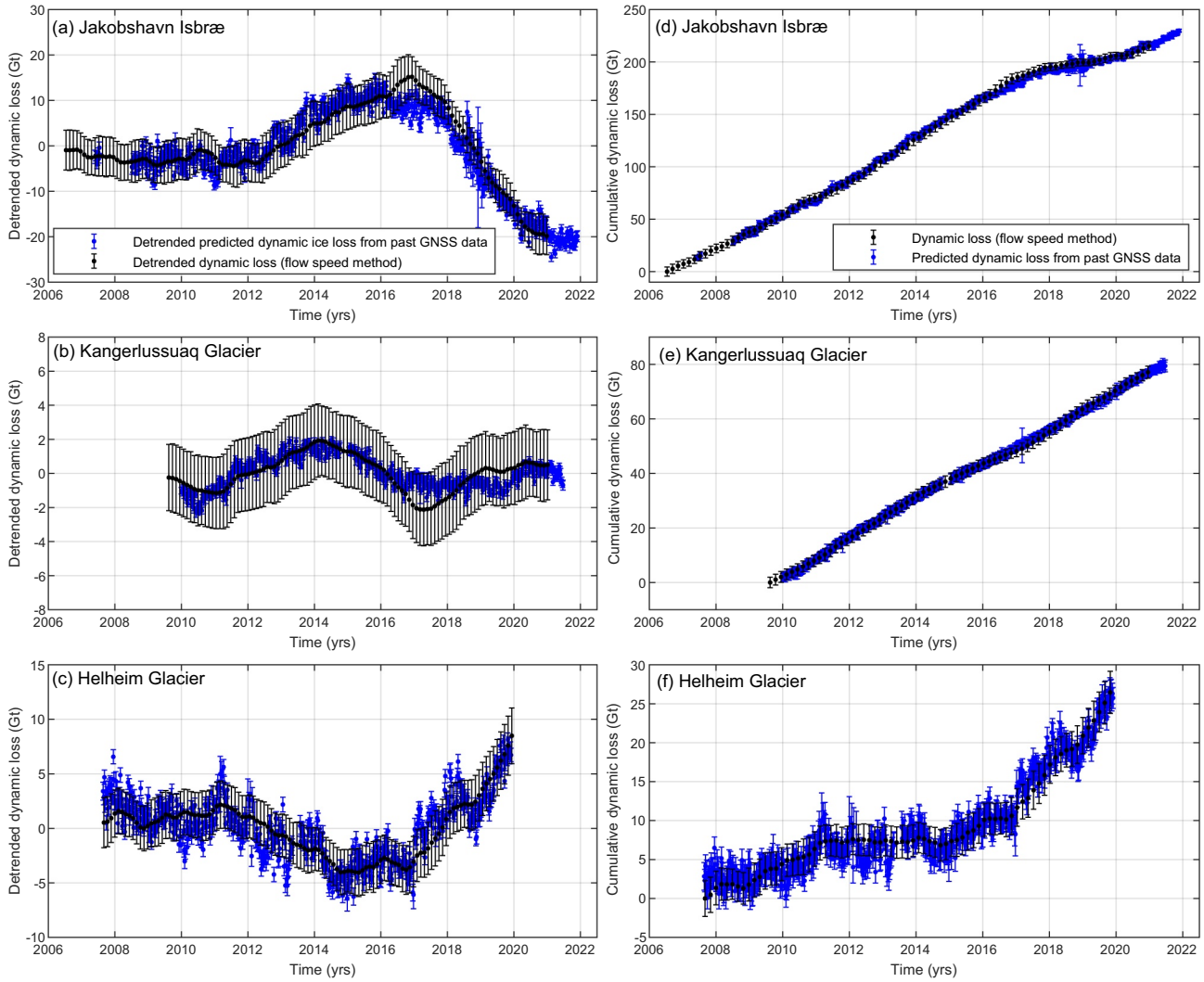

Figure 3. (a) Predicted detrended dynamic ice loss from past GNSS data at JI (blue curve) and ice flow method (black curve). (b) Same as (a) but for KG. (c) Same as (a) but for HG. (d) Cumulative dynamic ice loss from past GNSS data at JI (blue curve) and ice flow speed method (black curve). (e) Same as (d) but for KG. (f) Same as (d) but for HG.

where k is a constant that depends local geology and glaciohydrology and the distance between the GNSS site and the section of the glacier losing mass and has units of Gt/mm. t_0 is a constant time lag with units of years between detrended cumulative ice discharge $D(t)$ (Gt) and detrended cumulative bedrock uplift $U(t)$ (mm).

For each glacier, we estimate k and t_0 using least square adjustment. Figures 3a–3c shows time series of detrended dynamic ice loss from flow speed and detrended dynamic ice loss from GNSS using Equation 1. Table 1 shows our estimates of k and t_0 for JI, KG, and HG and their uncertainties (see Text S1).

Next, we use the detrended uplift time series $U(t)$ with associated parameters in Table 1 to reconstruct dynamic ice loss for JI, KG, and HG, respectively. Figures 3d–3f shows our reconstructed "dynamic ice loss from GNSS data" and "dynamic ice loss from ice flow speed." To reconstruct dynamic ice loss from GNSS uplift, we add the dynamic ice loss trend (see Table 1) that was removed when detrending dynamic ice loss time series in Figure 1 (right panels). Our method of estimating the relation between $U(t)$ and $D(t)$ and reconstruction of the dynamic ice loss from GNSS is independent of any secular trends that may affect GNSS data, for example, secular uplift due to glacial isostatic adjustment. Once a relation between uplift and dynamic ice loss has been established, we can use it to estimate dynamic ice loss from observed uplift

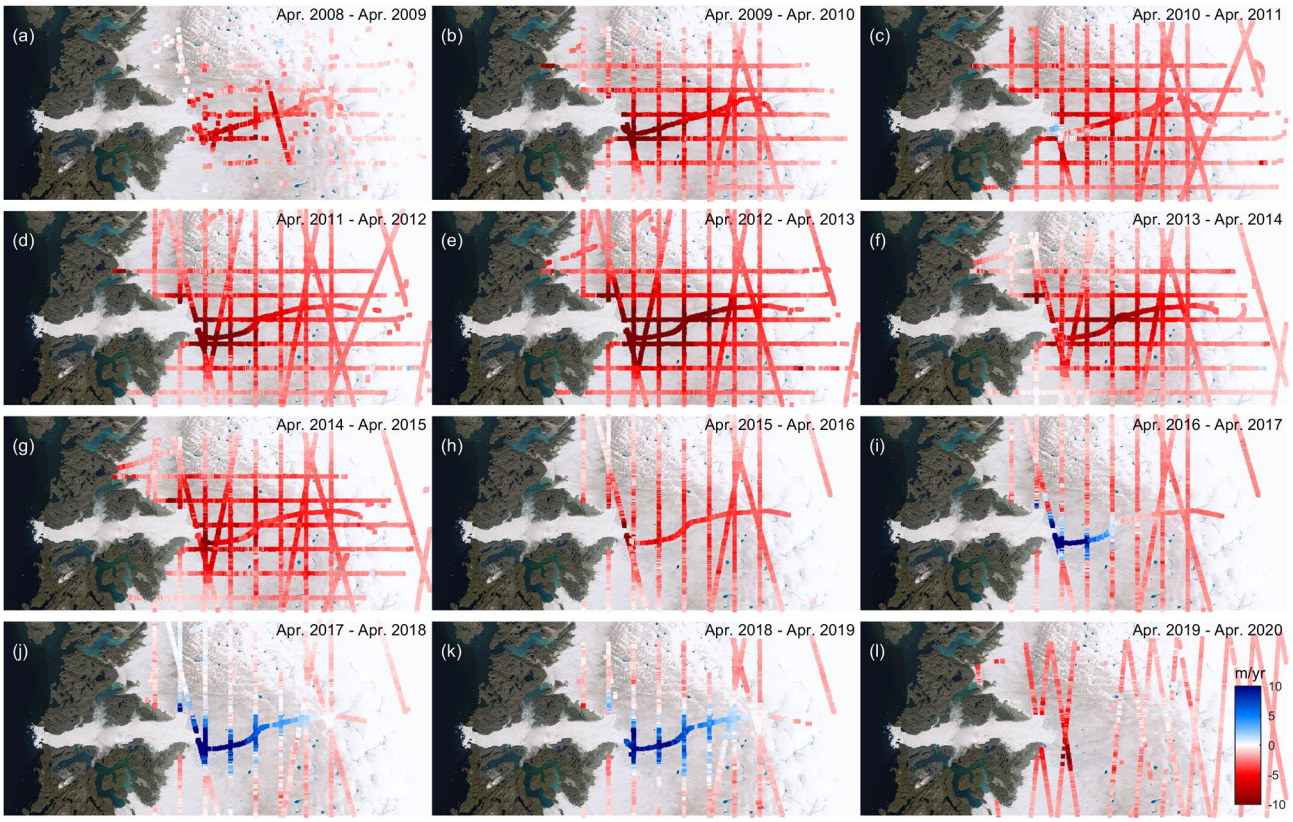

Figure 4. Elevation changes of Jakobshavn Isbræ in meters during (a) April 2008–April 2009, (b) April 2009–April 2010, (c) April 2010–April 2011, (d) April 2011–April 2012, (e) April 2012–April 2013, (f) April 2013–April 2014, (g) April 2014–April 2015, (h) April 2015–April 2016, (i) April 2016–April 2017, (j) April 2017–April 2018, (k) April 2018–April 2019, and (i) April 2019–April 2020. Background show Landsat image of JI from 2012.

from GNSS. In principle, the method can be used for any glacier that has a GNSS station located near the glacier terminus.

4. Results

The observed uplift at GNSS sites is an elastic response to mass changes due to a combination of complex patterns of SMB and dynamic induced response of JI, KG, and HG. By removing the SMB induced mass anomalies, we can isolate the dynamically-induced thinning. For each glacier, we find the relation between dynamic ice loss and uplift. Our results for HG (Figure 3f) show increased dynamic ice loss starting in 2017. HG lost a total of 10 ± 2 Gt during 2007.6–2017.0 (over a 9.4-year period) and 15 ± 2 Gt during 2017.0–2020.0 (over a 3-year period). Both methods, dynamic ice loss from flow speed and dynamic ice loss using GNSS, show acceleration in dynamic loss. The two methods provide consistent results for JI, KG, and HG, and the pairs of time-series (Figure 3) lie within their error bars. However, it should be noted that fluctuations in detrended dynamic ice loss are small for KG (from −2 to +2 Gt) (see Figure 3b), whereas JI fluctuations vary between −20 Gt and +10 Gt, and HG between −5 and +10 Gt.

In principle the time lag t_0 allows us to predict future dynamic loss from GNSS uplift. For JI we find a time lag of 0.87 ± 0.07 years between uplift and dynamic ice loss from flow speed, and thus we can predict dynamic ice loss until November 2021 (Figures 3a and 3d). The time lags for KG (0.37 ± 0.17 years, Figures 3b and 3e) and HG (0.03 ± 0.16 years, Figures 3c and 3f) are much shorter. To investigate and understand this time lag, we create time series of elevation changes for JI based on airborne and satellite laser altimetry data. Figure 4 shows annual elevation changes (April to April) from airborne and satellite altimetry between April 2008 and April 2020. The thinning is dominated by ice dynamics (Khazendar et al., 2019).

Airborne and satellite altimetry suggest thickening of JI from April 2016 to April 2017 (Figure 4i), in line with recent studies, for example, (Khazendar et al., 2019). However, discharge from flow speed shows a large decline in discharge in summer 2017 (Figure 1d) and was consistently lower the following years. This suggests a time lag between the onset of glacier speedup/slowdown and the onset of dynamic thinning/thickening, where dynamic thinning/thickening occurs before speedup/slowdown.

Our method of using GNSS uplift time series to estimate dynamic ice loss has its limitations. A GNSS station located between two glaciers will not be able to sense which glacier is speeding up and undergoing dynamic thinning/thickening. Elastic uplift depends on the distance between the GNSS site and the glacier losing mass. However, usage of horizontal displacements could be a potential solution, as horizontal displacements depend on the distance and direction between a GNSS site and the area losing mass (Adhikari et al., 2017; Wahr et al., 2013). The optimal location to install a GNSS station to monitor dynamic changes is close to the grounding line or close to the source that is, undergoing dynamic charges. A shorter distance between GNSS site and the source gives a larger elastic response.

5. Discussion and Conclusions

The Greenland GPS Network (GNET) was built to observe and monitor the Earth's instantaneous elastic adjustment to contemporary ice loss, and its delayed viscoelastic response to long past changes in ice mass (Bevis et al., 2012). Constant velocity displacements are hard to interpret, because both elastic and viscoelastic adjustments are capable of producing steady crustal velocities, so any attempt to separate them is largely an exercise in modeling. But accelerating and transient displacements are driven by accelerating or transient changes in ice mass, and thus manifest the combined effects of shifting SMB and dynamic mass change (Bevis et al., 2019). Changes in dynamic ice loss at major outlet glaciers produce large elastic signals at nearby GNSS stations, but these signals decay in space much more rapidly than do the signals produced by major shifts in SMB. Thus, displacement transients seen at GNET stations close to major outlet glaciers, which are not found in the time series of more distant GNET stations, have a local origin.

Here, we present a novel method to estimate dynamic ice loss of JI, KG, and HG that uses uplift from GNSS data. Our method provides weekly estimates of dynamic ice loss from 2007 to 2020 for JI and HG and 2009 to 2020 for KG (Figure 3). Our results show that uplift inferred from the GNSS data is a direct consequence of mass change with no time lag. The fact that the measured discharge at the flux gates lags the elastic response indicates that the ice flow at the flux gates reacts to dynamic thinning that has already occurred. This lag between glacier thinning/thickening and speedup/slowdown allows us to use uplift from GNSS data to predict discharge at the flux gates, by up to 10.4 months for JI and 4.5 months for KG.

One mechanism that we suggest leading to the lag is the delay of the viscous response to a change in load of a glacier. With ice being a viscoelastic material, a change in load is initially leading to an elastic response, while the viscous response is taking a month to years to fully develop, depending on the viscosity (Christmann et al., 2019; Rankl et al., 2017). Calving front motion induces softening of the ice that subsequently leads to acceleration (Bondzio et al., 2017). This implies that, locally, there might be a time lag between mass loss from the satellite altimetry method and the mass loss from the IOM method. Thus, on short timescales, the two mass loss methods should be compared with caution. We further note that the time lag between thinning/thickening and speedup/slowdown depends on the overall trend of the dynamic ice loss of the considered glacier. Table 1 suggests the time lag (column 3) increases linearly with the trend of dynamic ice loss (column 4). However, further investigation using more glaciers is needed to draw any conclusions. The method presented here may be used for other glaciers, for example, in Alaska or Antarctica that have a GNSS site located reasonably close (up to ~30 km) to their center of dynamic mass loss.

Data Availability Statement

Glacier front position and discharge data is available at the following data repository: https://dataverse01.geus.dk/dataset.xhtml?persistentId=doi:10.22008/promice/data/ice_discharge/d/v02.GNSS uplift data and Ice surface elevation changes is available at the following data repository: https://datadryad.org/stash/share/CTZfCRbKv3t3vEXloNHVdVycpFXza_yuBK38Lo6syDc.

Acknowledgments
The authors thank Jeffrey T. Freymueller and an anonymous reviewer for their constructive comments.
S. A. Khan acknowledges support from the INTAROS GA No. 727890 funded by European Union's Horizon 2020 Research and Innovation Programme. B. Noël was funded by the NWO VENI grant VI.Veni.192.019. A. Bjørk was funded by the Carlsberg Foundation (Grant CF17-0529). K. D. Mankoff was funded by PROMICE. M. R. van den Broeke acknowledges support from the Netherlands Earth System Science Centre (NESSC). W. Colgan acknowledges support from the Independent Research Fund Denmark (8049-00003B). A. Aschwanden was funded by NSF grant PLR-1603799.

References

Adhikari, S., Ivins, E. R., & Larour, E. (2017). Mass transport waves amplified by intense Greenland melt and detected in solid Earth deformation. *Geophysical Research Letters*, *44*(10), 4965–4975. https://doi.org/10.1002/2017gl073478

Altamimi, Z., Rebischung, P., Métivier, L., & Collilieux, X. (2016). ITRF2014: A new release of the International Terrestrial Reference Frame modeling nonlinear station motions. *Journal of Geophysical Research: Solid Earth*, *121*(8), 6109–6131. https://doi.org/10.1002/2016jb013098

Bamber, J. L., Westaway, R. M., Marzeion, B., & Wouters, B. (2018). The land ice contribution to sea level during the satellite era. *Environmental Research Letters*, *13*(6), 063008. https://doi.org/10.1088/1748-9326/aac2f0

Barletta, V. R., Sørensen, L. S., & Forsberg, R. (2013). Scatter of mass changes estimates at basin scale for Greenland and Antarctica. *The Cryosphere*, *7*(5), 1411–1432. https://doi.org/10.5194/tc-7-1411-2013

Bertiger, W., Bar-Sever, Y., Dorsey, A., Haines, B., Harvey, N., Hemberger, D., et al. (2020). GipsyX/RTGx, a new tool set for space geodetic operations and research. *Advances in Space Research*, *66*(3), 469–489. https://doi.org/10.1016/j.asr.2020.04.015

Bevis, M., Harig, C., Khan, S. A., Brown, A., Simons, F. J., Willis, M., et al. (2019). Accelerating changes in ice mass within Greenland, and the ice sheet's sensitivity to atmospheric forcing. *Proceedings of the National Academy of Sciences*, *116*(6), 1934–1939. https://doi.org/10.1073/pnas.1806562116

Bevis, M., Wahr, J., Khan, S. A., Madsen, F. B., Brown, A., Willis, M., et al. (2012). Bedrock displacements in Greenland manifest ice mass variations, climate cycles and climate change. *Proceedings of the National Academy of Sciences*, *109*(30), 1944–11948. https://doi.org/10.1073/pnas.1204664109

Boehm, J., Werl, B., & Schuh, H. (2006). Troposphere mapping functions for GPS and very long baseline interferometry from European Center for Medium-Range Weather Forecasts operational analysis data. *Journal of Geophysical Research: Solid Earth*, *111*(B2). B02406. https://doi.org/10.1029/2005jb003629

Bondzio, J. H., Morlighem, M., Seroussi, H., Kleiner, T., Rückamp, M., Mouginot, J., et al. (2017). The mechanisms behind Jakobshavn Isbræ's acceleration and mass loss: A 3-D thermomechanical model study. *Geophysical Research Letters*, *44*, 6252–6260. https://doi.org/10.1002/2017GL073309

Carrère, L., Lyard, F., Cancet, M., Guillot, A., & Picot, N. (2016). FES 2014, a new tidal model—Validation results and perspectives for improvements. In *Proceedings of the ESA living planet symposium* (pp. 9–13).

Chen, J. L., Wilson, C. R., & Tapley, B. D. (2006). Satellite gravity measurements confirm accelerated melting of Greenland ice sheet. *Science*, *313*(5795), 1958–1960. https://doi.org/10.1126/science.1129007

Christmann, J., Müller, R., & Humbert, A. (2019). On nonlinear strain theory for a viscoelastic material model and its implications for calving of ice shelves. *Journal of Glaciology*, *65*, 1–224. https://doi.org/10.1017/jog.2018.107

Helm, V., Humbert, A., & Miller, H. (2014). Elevation and elevation change of Greenland and Antarctica derived from CryoSat-2. *The Cryosphere*, *8*(4), 1539–1559. https://doi.org/10.5194/tc-8-1539-2014

Joughin, I., Smith, B. E., & Howat, I. M. (2018). A complete map of Greenland ice velocity derived from satellite data collected over 20 years. *Journal of Glaciology*, *64*(243), 1–11. https://doi.org/10.1017/jog.2017.73

Khan, S. A., Bjørk, A. A., Bamber, J. L., Morlighem, M., Bevis, M., Kjær, K. H., et al. (2020). Centennial response of Greenland's three largest outlet glaciers. *Nature Communications*, *11*, 5718. https://doi.org/10.1038/s41467-020-19580-5

Khan, S. A., Kjær, K. H., Bevis, M., Bamber, J. L., Wahr, J., Kjeldsen, K. K., et al. (2014). Sustained mass loss of the northeast Greenland ice sheet triggered by regional warming. *Nature Climate Change*, *4*(4), 292–299. https://doi.org/10.1038/nclimate2161

Khan, S. A., Kjeldsen, K. K., Kjær, K. H., Bevan, S., Luckman, A., Aschwanden, A., et al. (2014). Glacier dynamics at Helheim and Kangerdlugssuaq glaciers, southeast Greenland, since the Little Ice Age. *The Cryosphere*, *8*, 1497–1507. https://doi.org/10.5194/tc-8-1497-2014

Khan, S. A., Liu, L., Wahr, J., Howat, I., Joughin, I., van Dam, T., & Fleming, K. (2010). GPS measurements of crustal uplift near Jakobshavn Isbræ due to glacial ice mass loss. *Journal of Geophysical Research*, *115*, B09405. https://doi.org/10.1029/2010jb007490

Khan, S. A., Sasgen, I., Bevis, M., van Dam, T., Bamber, J. L., Wahr, J., et al. (2016). Geodetic measurements reveal similarities between post-Last Glacial Maximum and present-day mass loss from the Greenland ice sheet. *Science Advances*, *2*, e1600931. https://doi.org/10.1126/sciadv.1600931

Khazendar, A., Fenty, I. G., Carroll, D., Gardner, A., Lee, C. M., Fukumori, I., et al. (2019). Interruption of two decades of Jakobshavn Isbrae acceleration and thinning as regional ocean cools. *Nature Geoscience*, *12*(4), 277–283. https://doi.org/10.1038/s41561-019-0329-3

King, M. D., Howat, I. M., Candela, S. G., Noh, M. J., Jeong, S., Noël, B. P. Y., et al. (2020). Dynamic ice loss from the Greenland Ice Sheet driven by sustained glacier retreat. *Communications Earth & Environment*, *1*, 1. https://doi.org/10.1038/s43247-020-0001-2

Mankoff, K. D., Solgaard, A., Colgan, W., Ahlstrøm, A. P., Khan, S. A., & Fausto, R. S. (2020). Greenland Ice Sheet solid ice discharge from 1986 through March 2020. *Earth System Science Data*, *12*(2), 1367–1383. https://doi.org/10.5194/essd-12-1367-2020

Morlighem, M., Williams, C. N., Rignot, E., An, L., Arndt, J. E., Bamber, J. L., et al. (2017). BedMachine v3: Complete bed topography and ocean bathymetry mapping of Greenland from multi-beam echo sounding combined with mass conservation. *Geophysical Research Letters*, *44*, 11051–11061. https://doi.org/10.1002/2017gl074954

Mouginot, J., Rignot, E., Bjørk, A. A., Van den Broeke, M., Millan, R., Morlighem, M., et al. (2019). Forty-six years of Greenland Ice Sheet mass balance from 1972 to 2018. *Proceedings of the National Academy of Sciences*, *116*(19), 9239–9244. https://doi.org/10.1073/pnas.1904242116

Nghiem, S. V., Hall, D. K., Mote, T. L., Tedesco, M., Albert, M. R., Keegan, K., et al. (2012). The extreme melt across the Greenland ice sheet in 2012. *Geophysical Research Letters*, *39*(20). L20502. https://doi.org/10.1029/2012gl053611

Noël, B., van de Berg, W. J., Lhermitte, S., & van den Broeke, M. R. (2019). Rapid ablation zone expansion amplifies north Greenland mass loss. *Science Advances*, *5*(9), eaaw0123. https://doi.org/10.1126/sciadv.aaw0123

Noël, B., van de Berg, W. J., van Wessem, J. M., van Meijgaard, E., van As, D., Lenaerts, J. T. M., et al. (2018). Modeling the climate and surface mass balance of polar ice sheets using RACMO2-Part 1: Greenland (1958–2016). *The Cryosphere*, *12*, 811–831. https://doi.org/10.5194/tc-12-811-2018

Pritchard, H. D., Arthern, R. J., Vaughan, D. G., & Edwards, L. A. (2009). Extensive dynamic thinning on the margins of the Greenland and Antarctic ice sheets. *Nature*, *461*(7266), 971–975. https://doi.org/10.1038/nature08471

Rankl, M., Fürst, J. J., Humbert, A., & Braun, M. H. (2017). Dynamic changes on the Wilkins ice shelf during the 2006–2009 retreat derived from satellite observations. *The Cryosphere*, *11*, 1199–1211. https://doi.org/10.5194/tc-11-1199-2017

Rignot, E., & Kanagaratnam, P. (2006). Changes in the velocity structure of the Greenland Ice Sheet. *Science*, *311*(5763), 986–990. https://doi.org/10.1126/science.1121381

Sasgen, I., Wouters, B., Gardner, A. S., King, M. D., Tedesco, M., Landerer, F. W., et al. (2020). Return to rapid ice loss in Greenland and record loss in 2019 detected by the GRACE-FO satellites. *Communications Earth & Environment*, *1*(1), 1–8. https://doi.org/10.1038/s43247-020-0010-1

Schenk, T., Csatho, B., Van Der Veen, C., & McCormick, D. (2014). Fusion of multi-sensor surface elevation data for improved characterization of rapidly changing outlet glaciers in Greenland. *Remote Sensing of Environment*, *149*, 239–251. https://doi.org/10.1016/j.rse.2014.04.005

Shepherd, A., Ivins, E., Rignot, E., Smith, B., van Den Broeke, M., Velicogna, I., et al. (2020). Mass balance of the Greenland ice sheet from 1992 to 2018. *Nature*, *579*(7798), 233–239. https://doi.org/10.1038/s41586-019-1855-2

Smith, B., Fricker, H. A., Gardner, A., Siegfried, M. R., Adusumilli, S.,Csathó, B. M., et al. (2020). *ATLAS/ICESat-2 L3A land ice height, version 3. [2018–2020]*. NASA National Snow and Ice Data Center Distributed Active Archive Center. https://doi.org/10.5067/ATLAS/ATL06.003

Solgaard, A., Kusk, A., Boncori, J. P. M., Dall, J., Mankoff, K. D., Ahlstrøm, A. P., et al. (2021). Greenland ice velocity maps from the PROMICE project. *Earth System Science Data Discussions*, 1–29.

Studinger, M. (2014). *IceBridge ATM L2 Icessn elevation, slope, and roughness, version 2. [2011–2019]*. NASA National Snow and Ice Data Center Distributed Active Archive Center. Updated 2020. https://doi.org/10.5067/CPRXXK3F39RV

van den Broeke, M. R., Enderlin, E. M., Howat, I. M., Kuipers Munneke, P., Noël, B. P. Y., van de Berg, W. J., et al. (2016). On the recent contribution of the Greenland ice sheet to sea level change. *The Cryosphere*, *10*, 1933–1946. https://doi.org/10.5194/tc-10-1933-2016

Velicogna, I., & Wahr, J. (2006). Measurements of time-variable gravity show mass loss in Antarctica. *Science*, *311*(5768), 1754–1756. https://doi.org/10.1126/science.1123785

Wahr, J., Khan, S. A., van Dam, T., Liu, L., van Angelen, J. H., van den Broeke, M. R., & Meertens, C. M. (2013). The use of GPS horizontals for loading studies, with applications to northern California and southeast Greenland. *Journal of Geophysical Research: Solid Earth*, *118*, 1795–1806. https://doi.org/10.1002/jgrb.50104

Wang, H., Xiang, L., Jia, L., Jiang, L., Wang, Z., Hu, B., & Gao, P. (2012). Load Love numbers and Green's functions for elastic Earth models PREM, iasp91, ak135, and modified models with refined crustal structure from crust 2.0. *Computers & Geosciences*, *49*, 190–199. https://doi.org/10.1016/j.cageo.2012.06.022